

Harnessing Van der Waals CrPS₄ and Surface Oxides for Nonmonotonic Preset Field Induced Exchange Bias in Fe₃GeTe₂

Aravind Puthirath Balan,^{*,¶} Aditya Kumar,[¶] Tanja Scholz, Zhongchong Lin, Aga Shahee, Shuai Fu, Thibaud Denneulin, Joseph Vas, András Kovács, Rafal E. Dunin-Borkowski, Hai I. Wang, Jinbo Yang, Bettina V. Lotsch, Ulrich Nowak, and Mathias Kläui^{*}



Cite This: *ACS Nano* 2024, 18, 8383–8391



Read Online

ACCESS |



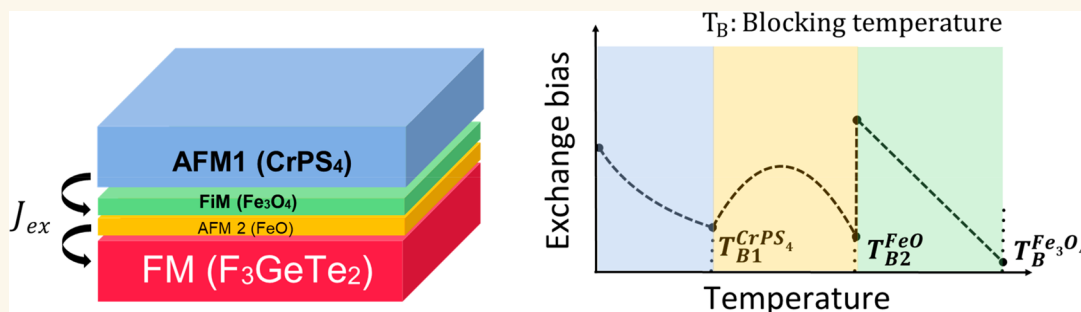
Metrics & More



Article Recommendations



Supporting Information



ABSTRACT: Two-dimensional van der Waals (vdW) heterostructures are an attractive platform for studying exchange bias due to their defect-free and atomically flat interfaces. Chromium thiophosphate (CrPS₄), an antiferromagnetic material, possesses uncompensated magnetic spins in a single layer, rendering it a promising candidate for exploring exchange bias phenomena. Recent findings have highlighted that naturally oxidized vdW ferromagnetic Fe₃GeTe₂ exhibits exchange bias, attributed to the antiferromagnetic coupling of its ultrathin surface oxide layer (O-FGT) with the underlying unoxidized Fe₃GeTe₂. Anomalous Hall measurements are employed to scrutinize the exchange bias within the CrPS₄/(O-FGT)/Fe₃GeTe₂ heterostructure. This analysis takes into account the contributions from both the perfectly uncompensated interfacial CrPS₄ layer and the interfacial oxide layer. Intriguingly, a distinct and nonmonotonic exchange bias trend is observed as a function of temperature below 140 K. The occurrence of exchange bias induced by a “preset field” implies that the prevailing phase in the polycrystalline surface oxide is ferrimagnetic Fe₃O₄. Moreover, the exchange bias induced by the ferrimagnetic Fe₃O₄ is significantly modulated by the presence of the van der Waals antiferromagnetic CrPS₄ layer, forming a heterostructure, along with additional iron oxide phases within the oxide layer. These findings underscore the intricate and complex nature of exchange bias in van der Waals heterostructures, highlighting their potential for tailored manipulation and control.

KEYWORDS: *vdW magnetic materials, exchange bias, vdW heterostructures, Fe₃GeTe₂, CrPS₄*

The phenomenon of exchange bias (EB) arises when a ferromagnetic (FM) material and an antiferromagnetic (AFM) material are brought into contact, resulting in the development of a unidirectional magnetic anisotropy at their interface.¹ This introduced anisotropy causes a shift in the magnetic hysteresis loop of FM along the field axis. EB has significant implications in various device technologies, such as spin valves, which find applications in high-density magnetic storage and sensor systems.² The underlying mechanism behind EB is generally attributed to the exchange coupling

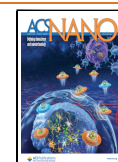
between uncompensated spins within the AFM and the FM moments across the interface.^{3,4} However, in thin-film heterostructures comprising non-van der Waals solids, the

Received: December 25, 2023

Revised: February 19, 2024

Accepted: February 28, 2024

Published: March 4, 2024



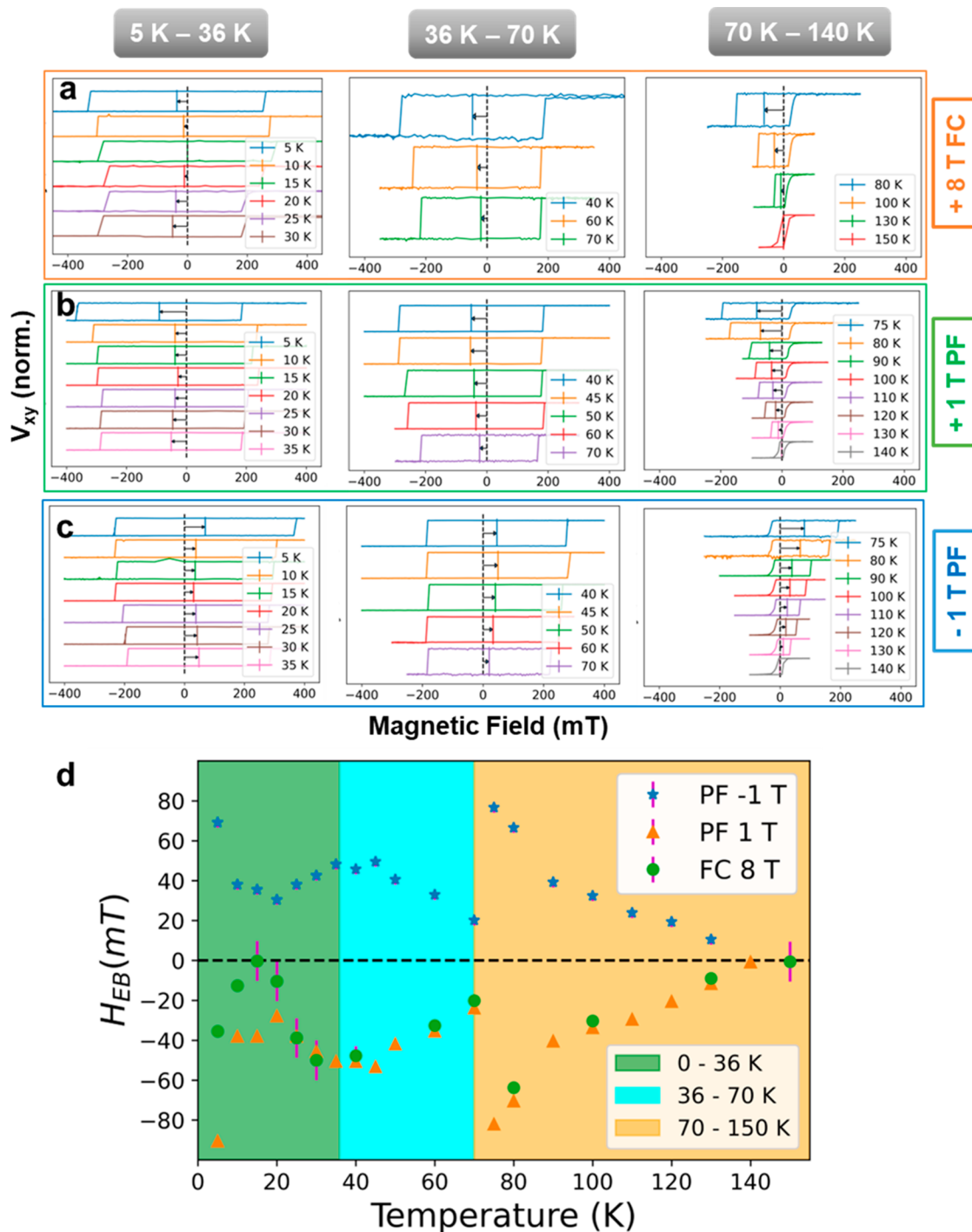


Figure 1. EB due to surface oxide layers formed at the $\text{CrPS}_4\text{-Fe}_3\text{GeTe}_2$ interface. Anomalous Hall voltage (V_{xy}) measured as a function of sweeping magnetic field for a $\text{CrPS}_4/(\text{O-FGT})/\text{Fe}_3\text{GeTe}_2$ with (a) +8 T field-cooling (FC), (b) +1 T preset field (PF), (c) -1 T preset field, and (d) trend of exchange bias field (H_{EB}) calculated as a function of temperature for both positive (orange) and negative (blue) 1 T preset field experiments as well as for the +8 T field-cooled experiments (green).

presence of imperfections like interdiffusion, step edges, grain boundaries, interfacial stress, and roughness can compromise the ideal interface quality.⁵

The recent emergence of van der Waals (vdW) magnetic materials exhibiting atomically smooth surfaces revitalized interest in understanding the microscopic origins of EB.⁶ With their inherent layered structure, vdW materials offer the potential to form heterostructures with nearly ideal interfaces, making them particularly promising for investigating interface-

related effects, especially pertaining to EB.⁷ Recent reports have unveiled the occurrence of EB in the vdW AFM/FM heterostructures. For instance, an EB of approximately 50 mT was identified in a $\text{CrCl}_3/\text{Fe}_3\text{GeTe}_2$ heterostructure at 2.5 K.⁸ Subsequent investigations involved various vdW AFM layers (MnPS_3 , MnPSe_3 , FePS_3) atop metallic Fe_3GeTe_2 or Fe_5GeTe_2 .^{9,10} A substantial EB was also observed in a heterostructure composed of a vdW FM insulator and an AFM topological insulator ($\text{CrI}_3/\text{MnBi}_2\text{Te}_4$) with partial

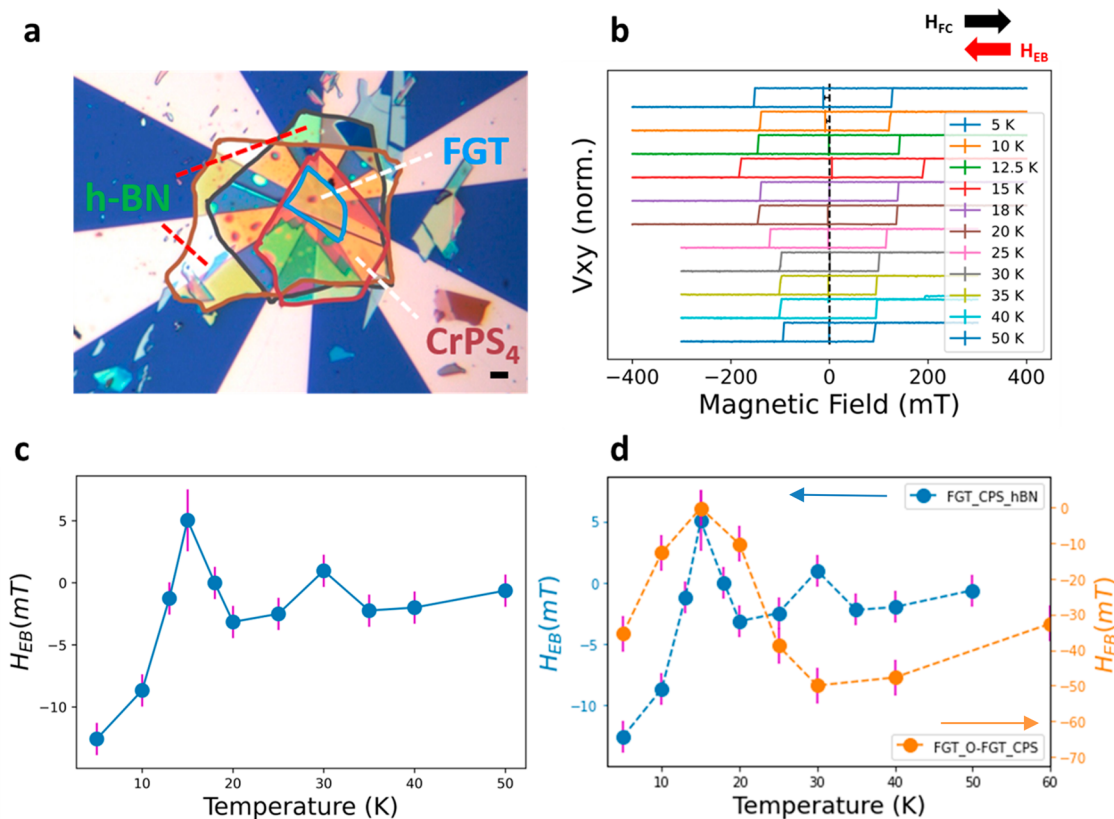


Figure 2. EB due to a pristine CrPS₄/Fe₃GeTe₂ interface. (a) Optical micrograph of a h-BN/CrPS₄/Fe₃GeTe₂ device (scale bar 10 μm). (b) Anomalous Hall voltage (V_{xy}) measured as a function of sweeping magnetic field for the capped device at various temperatures from 5 to 50 K for +8 T field-cooling (directions of H_{FC} and H_{EB} are indicated by black and red arrows, respectively). (c) The trend of H_{EB} as a function of temperature for +8 T field-cooling. (d) Comparison of H_{EB} for a pristine and for oxygen-exposed devices for +8T field-cooling.

coverage.¹¹ Another notable development is the observation of EB in naturally occurring superlattice structures of MnBi₂Te₄(Bi₂Te₃)_{*n*} (*n* = 1, 2), attributed to exchange coupling between coexisting ferromagnetic and antiferromagnetic constituents in the ground state.¹²

Among vdW AFMs, CrPS₄ stands out due to its fully uncompensated layered structure, enabling ideal coupling at the interface within vdW AFM/FM heterostructures.^{13–15} Moreover, Fe₃GeTe₂ (FGT) is an itinerant vdW ferromagnet boasting a substantial Curie temperature of 220 K in bulk.¹⁶ Recent investigations have highlighted that an air-exposed Fe₃GeTe₂ crystal naturally forms a thin antiferromagnetic surface oxide layer (O-FGT), resulting in EB in the underlying unoxidized crystal.¹⁷ Analytical techniques, including energy dispersive spectroscopy mapping, X-ray absorption spectroscopy, and electron energy loss spectroscopy have indicated a polycrystalline nature for the oxide layer, suggesting the presence of diverse phases such as FeO, Fe₂O₃, and Fe₃O₄ corresponding to varying Fe²⁺ and Fe³⁺ oxidation states.^{18,19} This surface oxide has also been found to enhance EB in CrOCl/Fe₃GeTe₂ heterostructures.²⁰ Notably, significant EB has been reported in naturally oxidized and restacked liquid exfoliated Fe₃GeTe₂ nanoflakes.²¹ Nevertheless, investigations elucidating the precise magnetic characteristics of the formed oxide layer and its role in introducing the EB remain lacking.

This study focuses on the characterization of EB properties within vdW heterostructures, specifically CrPS₄/(O-FGT)/Fe₃GeTe₂ and CrPS₄/Fe₃GeTe₂, using magneto-transport measurements. Our findings unveil the intricate magnetic

signatures underlying the observed robust EB in CrPS₄/(O-FGT)/Fe₃GeTe₂, which primarily stems from the dominance of ferrimagnetic magnetite within the surface oxide at the interface. Furthermore, we ascertain that the EB attributed to magnetite is influenced by the presence of vdW CrPS₄ in a heterostructure and the coexistence of a second antiferromagnetic iron oxide phase in the polycrystalline surface oxide. Through a comprehensive analysis of both the complex EB in CrPS₄/(O-FGT)/Fe₃GeTe₂ and the intrinsic EB in CrPS₄/Fe₃GeTe₂ featuring a pristine interface, this study provides insights into tailoring the EB in vdW heterostructures.

RESULTS AND DISCUSSIONS

Single crystals of Fe₃GeTe₂ and CrPS₄ are grown using chemical vapor transport following previous reports.^{22,23} The quality of synthesized crystals is examined by Raman spectroscopy (please refer to Figure S1 in the Supporting Information under Section 1). All the modes obtained for both Fe₃GeTe₂ and CrPS₄ bulk crystals match well with the predicted Raman modes.^{24,25} To explore the impact of the O-FGT layer on EB, two heterostructures are fabricated: CrPS₄/(O-FGT)/Fe₃GeTe₂ and CrPS₄/Fe₃GeTe₂. In the former, a surface oxide layer coats the surface of the Fe₃GeTe₂ flake at the interface, while the latter features a pristine Fe₃GeTe₂ surface. The surface oxide formation is confirmed using element-sensitive cross-sectional transmission electron microscopy measurements (please refer to Figure S2a–h in the Supporting Information under Section 2 for details) of a CrPS₄/(O-FGT)/Fe₃GeTe₂ heterostructure. The thickness of

the Fe_3GeTe_2 and CrPS_4 layers of the oxidized heterostructure is determined to be 30 and 100 nm, respectively, using atomic force microscopy (for details, please refer to Figure S3 in Supporting Information under Section 3). $\text{CrPS}_4/(\text{O-FGT})/\text{Fe}_3\text{GeTe}_2$ heterostructures are fabricated onto a pre-patterned anomalous Hall contacts and are subjected to magnetotransport anomalous Hall voltage (V_{xy}) measurements. Please refer to the Methods section for more details about the device fabrication and anomalous Hall voltage measurements. The results obtained are summarized in Figure 1. Exchange bias field (H_{EB}) is determined from V_{xy} measured as a function of sweeping magnetic field, $H_{\text{EB}} = \left(\frac{H_{\text{C}}^+ + H_{\text{C}}^-}{2}\right)$, where H_{C}^+ and H_{C}^- represent the coercivities at positive and negative fields, respectively.

Initially, we used a magnetic field of +8 T to cool the $\text{CrPS}_4/(\text{O-FGT})/\text{Fe}_3\text{GeTe}_2$ device from room temperature to the desired temperatures. Then, we determined the corresponding H_{EB} at these temperatures by analyzing V_{xy} measured as a function of the sweeping magnetic field. The process is repeated for several temperature set points from 5 K up to 150 K, and the results are summarized in Figure 1a. H_{EB} is calculated for all of them and plotted as a function of the temperature (Figure 1d). It is generally expected that the magnitude of H_{EB} is maximum at low temperatures and gradually decreases as we go to higher temperatures and disappears above the blocking temperature (T_{B}) of the AFM. However, the H_{EB} here follows a complex nonmonotonic trend with the temperature. As indicated by the curve in green circles in Figure 1d, the observed trend consists of three distinct regions (indicated by three different colors) characterized by two local minima at ~ 20 and ~ 70 K, respectively. The robust EB observed up to 140 K can be attributed to the surface oxide formation on Fe_3GeTe_2 at the interface, as previously reported.¹⁷ However, the complex trend with temperature that we observe has not been studied and reported before. To understand the mechanisms in the low temperature regime, i.e., 5 to 36 K, one needs to analyze the EB on a hexagonal boron nitride(h-BN) capped $\text{CrPS}_4/\text{Fe}_3\text{GeTe}_2$ device with a pristine interface without any oxide formation (please refer to the Methods section for details of device fabrication).

To analyze the EB of the device with a pristine interface (see Figure 2a for the optical image), the device is field-cooled from room temperature to temperatures below 36 K, the Néel temperature (T_{N}) of CrPS_4 , with an out-of-the-plane field of +8 T. After the field cooling, V_{xy} is measured as a function of sweeping magnetic field at various temperatures from 5 to 50 K, and the results are summarized in Figure 2b. The directions of cooling field (H_{FC}) and EB observed are indicated by black and red arrows, respectively. H_{EB} is calculated and plotted as a function of temperature (Figure 2c). At 5 K, the magnitude of H_{EB} for a $\text{CrPS}_4/\text{Fe}_3\text{GeTe}_2$ device with a pristine interface is found to be ~ 12.5 mT (± 1 mT), which gradually decreases as the temperature is increased and found to be negligible (< 2 mT) above 20 K, the T_{B} of CrPS_4 as reported previously.²² We also observed a switching of the polarity of EB from negative to positive at 15 K close to the T_{B} , similar to the observations by S. Ding et al., where they observed switching EB behavior in pristine $\text{CrPS}_4/\text{FeNi}$ interface.²²

Interestingly, the observed T_{B} for a $\text{CrPS}_4/\text{Fe}_3\text{GeTe}_2$ system is found to be 20 K, significantly lower than the T_{N} of CrPS_4 . An estimation of the interfacial exchange coupling energy between CrPS_4 and Fe_3GeTe_2 , calculated using a simplistic

model provided by D. Mauri et al.,²⁶ is comparable to the weaker interlayer antiferromagnetic exchange coupling (0.16 meV) in CrPS_4 .¹⁵ This indicates that the exchange field from Fe_3GeTe_2 can be as strong as the spin-flip field in CrPS_4 and potentially be even stronger as the temperature approaches T_{N} of CrPS_4 when the spin-flip field decreases.¹⁵ In the case of the pristine $\text{CrPS}_4/\text{Fe}_3\text{GeTe}_2$ system, at temperatures above 20 K, the exchange field may exceed the spin-flip field. Consequently, CrPS_4 would flip with Fe_3GeTe_2 , resulting in zero EB, thus explaining the lower T_{B} observed.

As shown in Figure 2d, the variation of H_{EB} for a $\text{CrPS}_4/(\text{O-FGT})/\text{Fe}_3\text{GeTe}_2$ (orange curve) follows a trend similar to that observed for a pristine $\text{CrPS}_4/\text{Fe}_3\text{GeTe}_2$ interface (blue curve), albeit with an enhanced magnitude. The enhancement in the magnitude of H_{EB} observed here is analogous to what has been observed previously in $\text{CrOCl}/(\text{O-FGT})/\text{Fe}_3\text{GeTe}_2$ heterostructures.²⁰ The presence of the O-FGT layer enhances the overall interface coupling strength, thereby increasing H_{EB} . However, a comparatively smaller uncompensated moment in the O-FGT layer couples weakly with the interfacial CrPS_4 layer. This may result in CrPS_4 retaining its antiferromagnetic state even above the observed T_{B} and can still induce EB up to T_{N} . Consequently, the magnitude of H_{EB} in $\text{CrPS}_4/(\text{O-FGT})/\text{Fe}_3\text{GeTe}_2$ increases from the minima at 15 K corresponding to the maximum positive EB in the pristine device up to T_{N} (CrPS_4) = 36 K (refer to Figure 2d) where the positive EB from CrPS_4 disappears. The second minimum at 70 K (Figure 1d) further suggests that two different phases in the surface oxide contribute to EB, which is consistent with previous reports.^{18,19} However, determining the exact nature of oxide phases is challenging, considering the polycrystalline nature of the surface oxide. Our investigation of EB in $\text{CrPS}_4/(\text{O-FGT})/\text{Fe}_3\text{GeTe}_2$ helps us unravel the nature of two distinct phases of oxides in O-FGT through their distinct EB fingerprints.

Surprisingly, unlike the $\text{CrPS}_4/\text{Fe}_3\text{GeTe}_2$ with a pristine interface, the $\text{CrPS}_4/(\text{O-FGT})/\text{Fe}_3\text{GeTe}_2$ device found to be generating EB even without field-cooling by merely applying a “preset field” (H_{PF}), and the H_{EB} due to ± 1 T preset field follows a similar trend as obtained for field-cooling (Figure 1d). Please see the Methods section for more information about H_{PF} and how it is different from conventional field-cooling. The V_{xy} measurements for $\text{CrPS}_4/(\text{O-FGT})/\text{Fe}_3\text{GeTe}_2$ corresponding to all three regions for both $H_{\text{PF}} = +1$ T, and $H_{\text{PF}} = -1$ T are summarized in Figure 1b and 1c, respectively. H_{EB} is calculated and plotted as a function of temperature (Figure 1d). Such a peculiar H_{PF} induced EB observed in $\text{CrPS}_4/(\text{O-FGT})/\text{Fe}_3\text{GeTe}_2$ heterostructure in the temperature range of 5 to 140 K suggests that the dominant phase in the O-FGT layer that contributes to EB could be ferrimagnetic Fe_3O_4 analogous to ferrimagnet generated EB reported previously.^{27,28} The dominance of ferrimagnetic Fe_3O_4 in the surface oxide layer is suggested, as its magnetic alignment in a particular direction by H_{PF} determines the direction of pinning and hence the direction of loop shift.²⁸

Material characterization techniques such as cross-sectional scanning transmission electron microscopy (STEM)—electron energy-loss spectroscopy (EELS) and surface sensitive X-ray photoelectron spectroscopy (XPS) (see Figure S4 and Figure S5 in the Supporting Information under Section 4 and Section 5, respectively) are performed to check possible phases of oxides in O-FGT. XPS $2p_{3/2}$ and $2p_{1/2}$ peaks suggest that the present oxide phases are Fe_3O_4 and Fe_2O_3 , with both Fe^{3+} and Fe^{2+} valence states. However, the analysis of the Fe-L3/L2

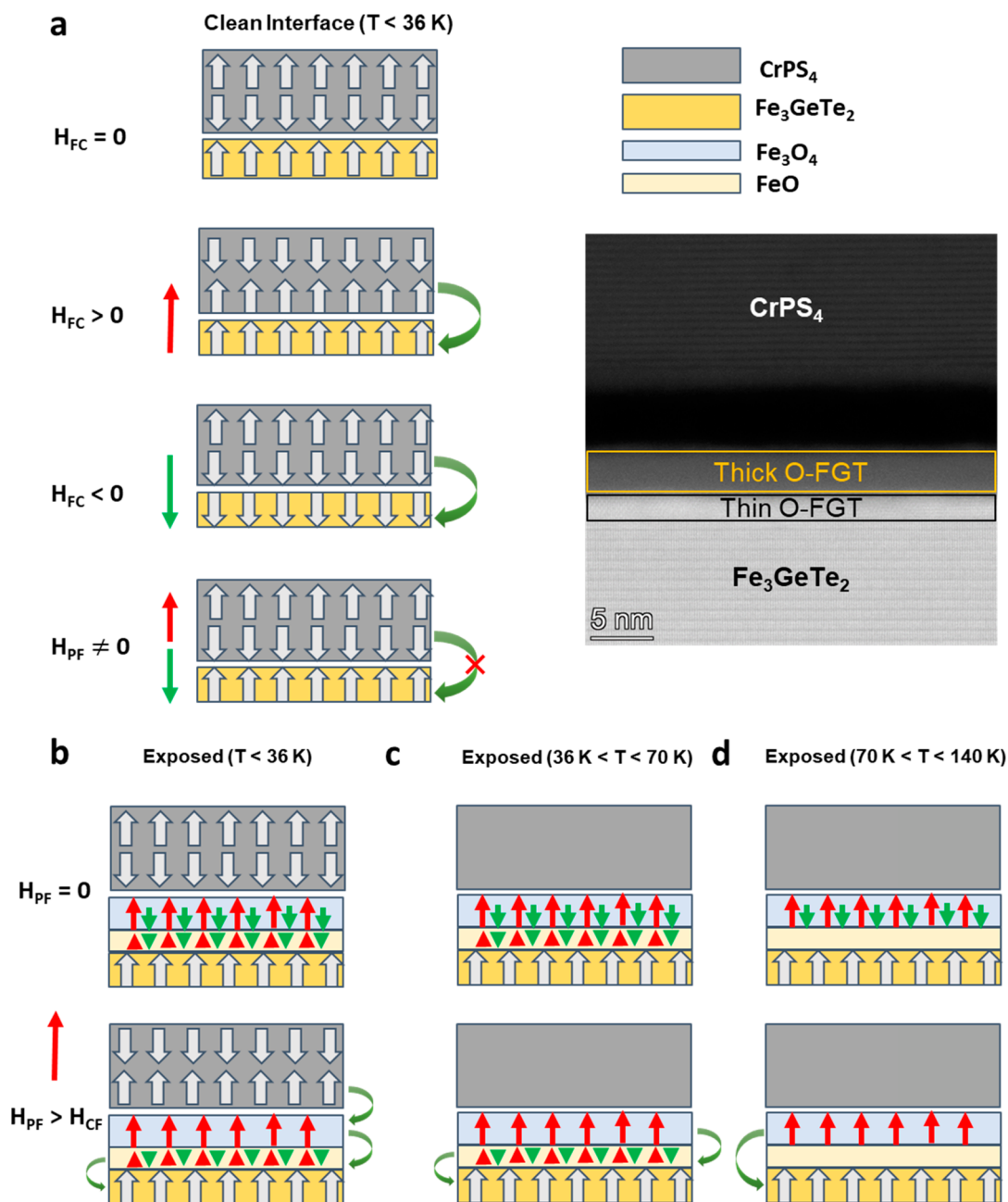


Figure 3. Schematic model. (a) Exchange coupling in a pristine interface CrPS₄/Fe₃GeTe₂ device after field-cooling (H_{FC}) with the cross-sectional STEM image of the CrPS₄/(O-FGT)Fe₃GeTe₂ in the inset, and the mechanism of exchange coupling induced by a preset field (H_{PF}) at different temperature ranges (b) $T < 36$ K, (c) 36 K $< T < 70$ K, and (d) $T > 70$ K. The out-of-plane positive and negative field directions are indicated by the long red and green arrows; the exchange coupling is indicated by curved arrows.

intensity ratio in EELS, in comparison with ratios obtained from spectra of reference samples, clearly suggests the presence of Fe₃O₄.¹⁹ The presence of Fe₃O₄ is further supported by the observation of a sudden increase in longitudinal resistance in an Fe₃GeTe₂ flake with an O-FGT layer at around 125 K, indicating a Verwey transition in Fe₃O₄ (see Figure S6a in the Supporting Information under Section 6).

Importantly, the minimum field required to saturate the ferrimagnetic Fe₃O₄ in the O-FGT at a particular temperature can be considered as the critical preset field (H_{CF}) for the system. Therefore, a H_{PF} greater than the H_{CF} in the preferred direction can be applied to judiciously determine the direction of EB (please refer to Figure S7 in Supporting Information

under Section 10). When the field is swept with a maximum value greater than H_{CF} at a given temperature preceded by a $H_{PF} \geq H_{CF}$, there is no preferred pinning by ferrimagnetic Fe₃O₄, resulting in zero EB (refer to Figure S8a–d in Supporting Information under Section 8).²⁸ In addition to Fe₃O₄, previous reports confirmed the presence of an antiferromagnetic FeO phase in the natural O-FGT.^{18,19} This coexisting FeO phase may have a low T_B of around 70 K, which is below the bulk $T_N = 198$ K.²⁹ The FeO phase is responsible for modulating the EB up to 70 K, where we observed a second minimum corresponding to the T_B of FeO (Figure 1d). Beyond 70 K, the EB is solely due to ferrimagnetic Fe₃O₄, which disappears at 140 K, the identified T_B .

Finally, the complex trend of H_{EB} with respect to the temperature can be understood based on an intuitive model of the contributions of CrPS_4 , as well as the two iron oxide phases in the O-FGT layer. The intuitive model is schematically represented in Figure 3. The various magnetic layers are color coded. The gray and yellow layers are the bottom and top layers of CrPS_4 and Fe_3GeTe_2 on either side of the vdW gap, whereas the O-FGT consists of effectively two layers: a thicker top layer mainly composed of Fe_3O_4 , as suggested by cross-sectional STEM-EELS measurements (for details, please refer to Figure S4 in Supporting Information under Section 4), and a thinner bottom layer composed of FeO , corresponding to the low valence state of Fe. The presence of two types of oxide layers is also evident from the different contrasts observed in the cross-sectional STEM image of the CrPS_4 /(O-FGT) Fe_3GeTe_2 interface (Figure 3a inset). In the case of the first device with a pristine interface, only a field-cooling below the T_N of CrPS_4 (36 K) can induce EB (Figure 3a), whereas it remains unbiased for H_{PF} (for details, please refer to Figure S9 in Supporting Information under Section 9). However, the reason for the observed positive EB close to T_B is still not understood properly. In the case of the second device with the O-FGT, however, three cases have to be considered as evident from Figure 1d: (i) $T < 36$ K (Figure 3b), where all the three constituents are magnetically ordered, (ii) 36 K $< T < 70$ K (Figure 3c), where CrPS_4 is paramagnetic, while both oxide phases are magnetically ordered, and (iii) 70 K $< T < 140$ K (Figure 3d), where only Fe_3O_4 is magnetically ordered, and contributes to EB since T_B of FeO is at 70 K.

Here, if we analyze the H_{EB} vs T (Figure 1d), it is apparent that the dominant contribution is due to ferrimagnetic Fe_3O_4 since we are observing H_{PF} induced EB (blue and orange curves) throughout the temperatures from 5 to 140 K. This is further reinforced by the absence of any EB due to pristine CrPS_4 after applying H_{PF} (for details, please refer to Figure S9 in Supporting Information under Section 9). However, CrPS_4 and FeO play important roles in modulating dominant EB due to Fe_3O_4 in the first two regions where they are magnetically ordered and their contributions to EB are evident. In the first case (Figure 3b), since all of the magnetic layers are in their magnetically ordered state, the resulting EB is then the net effect of all three EB contributions. The first local minimum of about ~ 20 K is identified as T_B of CrPS_4 . It is worth noting in Figure 1d that below 20 K, the influence of CrPS_4 on H_{EB} observed in a CrPS_4 /(O-FGT)/ Fe_3GeTe_2 device seems to be different for the measurements preceded by a conventional field-cooling (indicated by the green curve) and preceded by a H_{PF} (indicated by the blue and orange curves). H_{EB} is found to be large for 1 T preset-field more than what we obtained for an even higher cooling-field of 8 T (for detailed analysis, please refer to Figure S10 in the Supporting Information under Section 10). This suggests that in addition to modulation, a field-cooled CrPS_4 can have converse effects on the magnitude of H_{EB} , whereas CrPS_4 under H_{PF} application does not. Detailed spin structure information at a domain level is necessary to find out the underlying reason for this contrasting behavior, which is, however, beyond the scope of this investigation. Furthermore, a minor rise in $|H_{EB}|$ is observed, shifting from its minimum at 20 K to 36 K, mirroring the behavior observed after a field-cooling process, as previously discussed.

In the second case (Figure 3c), CrPS_4 is paramagnetic, and the net EB contribution could be the sum of the contributions

of Fe_3O_4 and FeO , with the second local minimum at 70 K corresponding to the T_B of FeO . Finally, above 70 K (Figure 3d), the EB contribution is only originating from ferrimagnetic Fe_3O_4 that acts directly as the source of pinning, however, through a thin and largely magnetically inactive spacer layer that mainly consists of FeO . This might weaken the longer distance exchange coupling, as evident by the significant training effect above 70 K (see Figure S11 in Supporting Information under Section 11). We observe that the H_{EB} , exclusively induced by Fe_3O_4 , is notably elevated at 80 K, exhibiting a comparable strength nearly equivalent to the H_{EB} observed at the significantly lower temperature of 5 K. This sudden increase in strength above 70 K is reasonable taking into account that the major pinning source is the Fe_3O_4 layer, which acts directly on the Fe_3GeTe_2 without any magnetically active intermediate layers, in contrast to the case where FeO is active below 70 K.

CONCLUSIONS

In summary, we have successfully demonstrated exchange bias in CrPS_4 /(O-FGT)/ Fe_3GeTe_2 vdW heterostructures, where we observed a complex nonmonotonic trend of exchange bias with temperature. The observed trend is apparent for both field-cooling as well as for a “preset field”. The two local minima observed in the exchange bias trend with the temperature are identified to correspond to the T_B of CrPS_4 and FeO . Saturating the ferrimagnetic Fe_3O_4 in the surface oxide by applying a field above a “critical preset field” determines the direction of the unidirectional exchange anisotropy and hence the direction of loop shift, which then allows us to tune the exchange bias. An intuitive model is proposed to explain the complex nonmonotonic trend of exchange bias fields as a function of temperature based on the different contributions. Our investigation identifies an alternative approach to tailor exchange bias in heterostructures by extrinsic methods such as oxidation combined with applied fields. We believe this investigation will motivate researchers to explore the exceptional tunability of magnetic properties in vdW heterostructures for spintronic applications. Given the large number of AFM vdW materials, our work provides insights into how surface oxide formation on the Fe_3GeTe_2 layer influences the exchange bias when interacting with other vdW antiferromagnets.

METHODS

A few layered flakes of Fe_3GeTe_2 and CrPS_4 were exfoliated onto Si/SiO₂ (300 nm) substrates using standard mechanical exfoliation with scotch tape. The bulk crystals were characterized employing Raman spectroscopy (please refer to Figure 1 in the Supporting Information under Section 1). Suitable flakes of uniform thickness were located using an optical microscope. The located Fe_3GeTe_2 and CrPS_4 flakes were picked up and transferred in the order mentioned, by typical polymer based dry transfer method, to prepatterned Hall contacts of Au/Cr (25 nm/5 nm) on Si/SiO₂ (300 nm) fabricated employing standard e-beam lithography. In order to investigate the impact of the surface oxide formed at the FM/AFM interface on EB, the surface of Fe_3GeTe_2 was exposed to an ambient atmosphere for 30 min before transferring the CrPS_4 layer resulting in the formation of an ultrathin oxide layer, which is referred to as (O-FGT). To compare, another CrPS_4 / Fe_3GeTe_2 heterostructure with a pristine interface was fabricated, the process of which was completely carried out inside the glovebox, containing an inert atmosphere (argon gas), and oxygen and moisture levels were kept below 0.5 ppm to make sure there is no effect of any oxidation. The fabricated device with a pristine interface

was then capped by hexagonal boron nitride (h-BN) flakes to prevent any chances of oxidation in air during device manipulation. The surface oxide formation was confirmed using element-sensitive cross-sectional transmission electron microscopy measurements (please refer to Figure 2 in Supporting Information under Section 2 for details) of an exposed and annealed Fe_3GeTe_2 flake with a CrPS_4 flake stamped on top afterward (Figure S2a–h). The thickness of the FM and AFM layers of the exposed heterostructure was determined to be 30 ± 2 nm and 100 ± 2 nm, respectively, using atomic force microscope, whereas it was found to be 33.3 ± 11.2 nm and 43.7 ± 9.8 nm for the capped device (please refer to Figure S3 in Supporting Information under Section 3). Both devices with pristine and exposed interfaces were then wire-bonded and immediately loaded onto a variable temperature insert (VTI) cryostat, in which we can apply a magnetic field up to 12 T for anomalous Hall effect measurements. Since CrPS_4 is an insulating antiferromagnet, the current will only flow through the metallic FGT layer. The cross-sectional area of the current channel ($10 \mu\text{m} \times 5 \mu\text{m}$) is $1.5 \times 10^{-13} \text{ m}^2$, and is used to calculate the current density, which is approximately $6.7 \times 10^6 \text{ Am}^{-2}$ along a 30 nm Fe_3GeTe_2 flake for an applied current of $1 \mu\text{A}$.

A $1 \mu\text{A}$ current was passed through the Fe_3GeTe_2 flake along the x -direction and the anomalous Hall voltage (V_{xy}) was measured across the transverse terminals along y -direction. The field was applied always with the OOP orientation for field-cooling, for field sweeping, and for application of a preset field (see below). A Keithley 2400 source meter was used to flow current through the device, and Keithley 2182a nanovoltmeter was used to measure voltage.

Preset Field (H_{PF}). The preset field, which is an out-of-plane field, is the field to which the device was exposed at a specific temperature just before starting the measurement of transverse anomalous Hall voltage (V_{xy}). It is important to note that the preset field and field cooling are different because preset field does not involve any cooling process through the T_{N} of the antiferromagnet. The mechanism of how a preset field determines the direction of pinning, and hence the direction of loop shift, is provided in Figure S7 under Supporting Information Section 7.

ASSOCIATED CONTENT

Supporting Information

The Supporting Information is available free of charge at <https://pubs.acs.org/doi/10.1021/acsnano.3c13034>.

Material morphology and structural characterization measurements conducted using Raman spectroscopy, transmission electron microscopy, X-ray photoelectron spectroscopy, and atomic force microscope techniques (Sections 1–5); Further transport measurements are included as supporting evidence for the observed phenomena discussed in the manuscript (Section 6 and Sections 8–11); Schematic diagram illustrating how a preset field induces exchange bias (Section 7) (PDF)

AUTHOR INFORMATION

Corresponding Authors

Aravind Puthirath Balan – *Institute of Physics, Johannes Gutenberg University Mainz, 55128 Mainz, Germany*; orcid.org/0000-0002-8272-1156; Email: aravindputhirath@uni-mainz.de

Mathias Kläui – *Institute of Physics, Johannes Gutenberg University Mainz, 55128 Mainz, Germany*; *Centre for Quantum Spintronics, Department of Physics, Norwegian University of Science and Technology, 7491 Trondheim, Norway*; orcid.org/0000-0002-4848-2569; Email: klaeui@uni-mainz.de

Authors

Aditya Kumar – *Institute of Physics, Johannes Gutenberg University Mainz, 55128 Mainz, Germany*

Tanja Scholz – *Max Planck Institute for Solid State Research, 70569 Stuttgart, Germany*; orcid.org/0000-0003-3474-1272

Zhongchong Lin – *State Key Laboratory for Artificial Microstructure and Mesoscopic Physics, School of Physics, Peking University, Beijing 100871, China*; orcid.org/0000-0001-9861-493X

Aga Shahee – *Institute of Physics, Johannes Gutenberg University Mainz, 55128 Mainz, Germany*; Present Address: Scientist-D/Ramanujan Fellow, Frontier Research Institute for Interdisciplinary Sciences (FRIIS), Islamic University of Science and Technology (IUST), Awantipora, J&K 192122, India; orcid.org/0000-0003-3860-1648

Shuai Fu – *Max Planck Institute for Polymer Research Mainz, 55128 Mainz, Germany*; Present Address: Research Associate, Chair for Molecular Functional Materials, TU Dresden, Walther-Hempel-Bau, Mommsenstraße 4 01069 Dresden, Germany; orcid.org/0000-0003-4038-2384

Thibaud Denneulin – *Ernst Ruska-Centre for Microscopy and Spectroscopy with Electrons, Peter Grünberg Institute, 52425 Jülich, Germany*

Joseph Vas – *Ernst Ruska-Centre for Microscopy and Spectroscopy with Electrons, Peter Grünberg Institute, 52425 Jülich, Germany*

András Kovács – *Ernst Ruska-Centre for Microscopy and Spectroscopy with Electrons, Peter Grünberg Institute, 52425 Jülich, Germany*; orcid.org/0000-0001-8485-991X

Rafal E. Dunin-Borkowski – *Ernst Ruska-Centre for Microscopy and Spectroscopy with Electrons, Peter Grünberg Institute, 52425 Jülich, Germany*; orcid.org/0000-0001-8082-0647

Hai I. Wang – *Max Planck Institute for Polymer Research Mainz, 55128 Mainz, Germany*; orcid.org/0000-0003-0940-3984

Jinbo Yang – *State Key Laboratory for Artificial Microstructure and Mesoscopic Physics, School of Physics, Peking University, Beijing 100871, China*; orcid.org/0000-0003-3517-9701

Bettina V. Lotsch – *Max Planck Institute for Solid State Research, 70569 Stuttgart, Germany*; orcid.org/0000-0002-3094-303X

Ulrich Nowak – *Department of Physics, University of Konstanz, 78464 Konstanz, Germany*

Complete contact information is available at: <https://pubs.acs.org/doi/10.1021/acsnano.3c13034>

Author Contributions

[¶]APB and AK contributed equally. APB, AK, and MK conceived the idea, design, and carried out the experiment. TS and BL synthesized the Fe_3GeTe_2 bulk crystals used for the experiments. ZCL and JY synthesized CrPS_4 single crystals. SF and HW performed Raman measurements. TD, JV, AKV, and RDB carried out the STEM measurements. AS and UN helped in interpretation of the results. All the authors contributed to manuscript writing.

Notes

A preprint version of this manuscript has been submitted in arXiv: Aravind Puthirath Balan, Aditya Kumar, Tanja Scholz,

Zhongchong Lin, Aga Shahee, Shuai Fu, Thibaud Denneulin, Joseph Vas, András Kovács, Rafal E. Dunin-Borkowski, Hai I. Wang, Jinbo Yang, Bettina Lotsch, Ulrich Nowak, Mathias Kläui. Harnessing van der Waals CrPS₄ and Surface Oxides for nonmonotonic preset field induced Exchange Bias in Fe₃GeTe₂. *arXiv*, March 23, 2023. DOI: [10.48550/arXiv.2303.13167](https://doi.org/10.48550/arXiv.2303.13167) (accessed on February 19, 2024). The authors declare no competing financial interest.

ACKNOWLEDGMENTS

We acknowledge funding from the Alexander von Humboldt Foundation for a Humboldt Postdoctoral Fellowship (Grant number: ref 3.5-IND-1216986-HFST-P), EU Marie-Curie Postdoctoral Fellowship ExBiaVdW (Grand Id: 101068014), Deutsche Forschungsgemeinschaft (DFG, German Research Foundation) – Spin + X TRR 173-268565370 (Projects No. A01 and No. B02), DFG Project No. 358671374, Graduate School of Excellence Materials Science in Mainz (MAINZ) GSC 266, the MaHoJeRo (DAAD Spintronics network, Projects No. 57334897 and No. 57524834), the Research Council of Norway (Centre for Quantum Spintronics – QuSpin No. 262633), the National Natural Science Foundation of China (Nos. 12241401 and 11975035), and the European Union's Horizon 2020 Research and Innovation Programme under grant agreement 856538 (project “3D MAGIC”). SF acknowledges the China Scholarship Council for financial support.

ABBREVIATIONS

EB	Exchange Bias
H_{EB}	Exchange Bias Field
V_{xy}	Anomalous Hall Voltage
H_{PF}	Preset Field
T_B	Blocking Temperature
T_N	Néel Temperature
O-FGT	Oxide layer formed on Fe ₃ GeTe ₂ flakes

REFERENCES

- Blachowicz, T.; Ehrmann, A. Exchange Bias in Thin Films—An Update. *Coatings* **2021**, *11*, 122.
- Coehoorn, R. Giant magnetoresistance and magnetic interactions in exchange-biased spin-valves. In *Handbook of Magnetic Materials*; Elsevier, 2003; Vol. 15, pp 1–197.
- Schuller, I. K.; Morales, R.; Battle, X.; Nowak, U.; Güntherodt, G. Role of the antiferromagnetic bulk spins in exchange bias. *J. Magn. Mater.* **2016**, *416*, 2–9.
- Nogués, J.; Schuller, I. K. Exchange bias. *J. Magn. Mater.* **1999**, *192*, 203–232.
- Fernando, G. W. Chapter 4: Magnetic Anisotropy in Transition Metal Systems. In *Handbook of Metal Physics*; Fernando, G. W., Ed.; Elsevier, 2008; Vol. 4, pp 89–110.
- Gong, C.; Zhang, X. Two-dimensional magnetic crystals and emergent heterostructure devices. *Science* **2019**, *363*, No. eaav4450.
- Phan, M.-H.; Kalappattil, V.; Jimenez, V. O.; Thi Hai Pham, Y.; Mudiyansele, N. W. Y. A. Y.; Detellem, D.; Hung, C.-M.; Chanda, A.; Eggers, T. Exchange bias and interface-related effects in two-dimensional van der Waals magnetic heterostructures: Open questions and perspectives. *J. Alloys Compd.* **2023**, *937*, 168375.
- Zhu, R.; Zhang, W.; Shen, W.; Wong, P. K. J.; Wang, Q.; Liang, Q.; Tian, Z.; Zhai, Y.; Qiu, C.-w.; Wee, A. T. S. Exchange Bias in van der Waals CrCl₃/Fe₃GeTe₂ Heterostructures. *Nano Lett.* **2020**, *20*, 5030–5035.
- Dai, H.; Cheng, H.; Cai, M.; Hao, Q.; Xing, Y.; Chen, H.; Chen, X.; Wang, X.; Han, J.-B. Enhancement of the Coercive Field and Exchange Bias Effect in Fe₃GeTe₂/MnPX₃ (X = S and Se) van der Waals Heterostructures. *ACS Appl. Mater. Interfaces* **2021**, *13*, 24314–24320.
- Albarakati, S.; Xie, W. Q.; Tan, C.; Zheng, G.; Algarni, M.; Li, J.; Partridge, J.; Spencer, M. J. S.; Farrar, L.; Xiong, Y.; et al. Electric Control of Exchange Bias Effect in FePS₃-Fe₅GeTe₂ van der Waals Heterostructures. *Nano Lett.* **2022**, *22*, 6166–6172.
- Ying, Z.; Chen, B.; Li, C.; Wei, B.; Dai, Z.; Guo, F.; Pan, D.; Zhang, H.; Wu, D.; Wang, X.; et al. Large Exchange Bias Effect and Coverage-Dependent Interfacial Coupling in CrI₃/MnBi₂Te₄ van der Waals Heterostructures. *Nano Lett.* **2023**, *23*, 765–771.
- Xu, X.; Yang, S.; Wang, H.; Guzman, R.; Gao, Y.; Zhu, Y.; Peng, Y.; Zang, Z.; Xi, M.; Tian, S.; et al. Ferromagnetic-antiferromagnetic coexisting ground state and exchange bias effects in MnBi₄Te₇ and MnBi₆Te₁₀. *Nat. Commun.* **2022**, *13*, 7646.
- Bo, X.; Li, F.; Yin, X.; Chen, Y.; Wan, X.; Pu, Y. Magnetic structure and exchange interactions of the van der Waals CrPS₄ monolayer under strain: A first-principles study. *Phys. Rev. B* **2023**, *108*, 024405.
- Calder, S.; Haglund, A. V.; Liu, Y.; Pajeroski, D. M.; Cao, H. B.; Williams, T. J.; Garlea, V. O.; Mandrus, D. Magnetic structure and exchange interactions in the layered semiconductor CrPS₄. *Phys. Rev. B* **2020**, *102*, 024408.
- Peng, Y.; Ding, S.; Cheng, M.; Hu, Q.; Yang, J.; Wang, F.; Xue, M.; Liu, Z.; Lin, Z.; Avdeev, M.; Hou, Y.; Yang, W.; Zheng, Y.; Yang, J. Magnetic structure and metamagnetic transitions in the van der Waals antiferromagnet CrPS₄. *Adv. Mater.* **2020**, *32*, 2001200.
- Fei, Z.; Huang, B.; Malinowski, P.; Wang, W.; Song, T.; Sanchez, J.; Yao, W.; Xiao, D.; Zhu, X.; May, A. F.; et al. Two-dimensional itinerant ferromagnetism in atomically thin Fe₃GeTe₂. *Nat. Mater.* **2018**, *17*, 778–782.
- Gweon, H. K.; Lee, S. Y.; Kwon, H. Y.; Jeong, J.; Chang, H. J.; Kim, K.-W.; Qiu, Z. Q.; Ryu, H.; Jang, C.; Choi, J. W. Exchange Bias in Weakly Interlayer-Coupled van der Waals Magnet Fe₃GeTe₂. *Nano Lett.* **2021**, *21*, 1672–1678.
- Kim, D. S.; Kee, J. Y.; Lee, J.-E.; Liu, Y.; Kim, Y.; Kim, N.; Hwang, C.; Kim, W.; Petrovic, C.; Lee, D. R.; et al. Surface oxidation in a van der Waals ferromagnet Fe₃-xGeTe₂. *Curr. Appl. Phys.* **2021**, *30*, 40–45.
- Li, Y.; Hu, X.; Fereidouni, A.; Basnet, R.; Pandey, K.; Wen, J.; Liu, Y.; Zheng, H.; Churchill, H. O. H.; Hu, J.; et al. Visualizing the Effect of Oxidation on Magnetic Domain Behavior of Nanoscale Fe₃GeTe₂ for Applications in Spintronics. *ACS Appl. Nano Mater.* **2023**, *6*, 4390–4397.
- Zhang, T.; Zhang, Y.; Huang, M.; Li, B.; Sun, Y.; Qu, Z.; Duan, X.; Jiang, C.; Yang, S. Tuning the Exchange Bias Effect in 2D van der Waals Ferro-/Antiferromagnetic Fe₃GeTe₂/CrOCl Heterostructures. *Adv. Sci.* **2022**, *9*, 2105483.
- Ma, S.; Li, G.; Li, Z.; Zhang, Y.; Lu, H.; Gao, Z.; Wu, J.; Long, G.; Huang, Y. 2D magnetic semiconductor Fe₃GeTe₂ with few and single layers with a greatly enhanced intrinsic exchange bias by liquid-phase exfoliation. *ACS Nano* **2022**, *16*, 19439–19450.
- Ding, S.; Peng, Y.; Xue, M.; Liu, Z.; Liang, Z.; Yang, W.; Sun, Y.; Zhao, J.; Wang, C.; Liu, S.; et al. Magnetic phase diagram of CrPS₄ and its exchange interaction in contact with NiFe. *J. Phys.: Condens. Matter* **2020**, *32*, 405804.
- Och, M.; Martin, M.-B.; Dlubak, B.; Seneor, P.; Mattevi, C. Synthesis of emerging 2D layered magnetic materials. *Nanoscale* **2021**, *13*, 2157–2180.
- Kong, X.; Berlijn, T.; Liang, L. Thickness and Spin Dependence of Raman Modes in Magnetic Layered Fe₃GeTe₂. *Adv. Electron. Mater.* **2021**, *7*, 2001159.
- Wu, H.; Chen, H. Probing the properties of lattice vibrations and surface electronic states in magnetic semiconductor CrPS₄. *RSC Adv.* **2019**, *9*, 30655–30658.
- Mauri, D.; Siegmann, H. C.; Bagus, P. S.; Kay, E. Simple model for thin ferromagnetic films exchange coupled to an antiferromagnetic substrate. *J. Appl. Phys.* **1987**, *62*, 3047–3049.

- (27) Radu, F.; Abrudan, R.; Radu, I.; Schmitz, D.; Zabel, H. Perpendicular exchange bias in ferrimagnetic spin valves. *Nat. Commun.* **2012**, *3*, 715.
- (28) Dho, J. Magnetic-field-induced switchable exchange bias in NiFe film on (110) Fe₃O₄ with a strong uniaxial magnetic anisotropy. *Appl. Phys. Lett.* **2015**, *106*, 202405.
- (29) Koziol-Rachwał, A.; Słęczak, T.; Nozaki, T.; Yuasa, S.; Korecki, J. Growth and magnetic properties of ultrathin epitaxial FeO films and Fe/FeO bilayers on MgO(001). *Appl. Phys. Lett.* **2016**, *108*, 041606.